

ACCEPTED MANUSCRIPT • OPEN ACCESS

Stability Evaluation and Mitigation Strategies in Advanced Tokamaks using 3D MHD Spectroscopy

To cite this article before publication: SeongMoo Yang et al 2025 Nucl. Fusion in press https://doi.org/10.1088/1741-4326/adf6c9

Manuscript version: Accepted Manuscript

Accepted Manuscript is "the version of the article accepted for publication including all changes made as a result of the peer review process, and which may also include the addition to the article by IOP Publishing of a header, an article ID, a cover sheet and/or an 'Accepted Manuscript' watermark, but excluding any other editing, typesetting or other changes made by IOP Publishing and/or its licensors"

This Accepted Manuscript is © 2025 The Author(s). Published by IOP Publishing Ltd on behalf of the IAEA.

As the version of Record of this article is going to be / has been published on a gold open access basis under a CC BY 4.0 licence, this Accepted Manuscript is available for reuse under a CC BY 4.0 licence immediately.

Everyone is permitted to use all or part of the original content in this article, provided that they adhere to all the terms of the licence https://creativecommons.org/licences/by/4.0

Although reasonable endeavours have been taken to obtain all necessary permissions from third parties to include their copyrighted content within this article, their full citation and copyright line may not be present in this Accepted Manuscript version. Before using any content from this article, please refer to the Version of Record on IOPscience once published for full citation and copyright details, as permissions may be required. All third party content is fully copyright protected and is not published on a gold open access basis under a CC BY licence, unless that is specifically stated in the figure caption in the Version of Record.

View the <u>article online</u> for updates and enhancements.

S.M. Yang¹, S. Munaretto¹, T. Liu², Q. Hu¹, C. Holcomb³, N.C. Logan⁴, B. Victor³, K. Ericksen¹, A. Bortolon¹

 Princeton Plasma Physics Laboratory, Princeton, New Jersey 08543, USA
Key Laboratory of materials Modification by Beams of the Ministry of Education, School of Physics, Dalian University of Technology, Dalian 116024, China
Lawrence Livermore National Laboratory, Irvine, California 94550, USA
Columbia University, New York, New York 10027, USA

E-mail: syang@pppl.gov

31 July 2025

Abstract. Multi-modal, active 3D MHD spectroscopy is applied in highperformance advanced tokamak scenarios to study their stability time evolution, revealing an intriguing dependence on both q_{min} and β_N . A tailored applied 3D field provides a 3D plasma response to extract the growth rate of the least stable mode. The estimated growth rate finds a decrease in stability when the minimum in the safety factor (q) passes through 2.0 and reveals inherent risks of crossing an additional rational surface at integer q_{min} , even above the usual q = 1 sawtooth condition. Based on this result, the potential scenario in which $q_{min} \sim 2$ can be safely crossed during a more stable lower β_N phase was investigated, and the improved stability of this scenario is confirmed by the estimated growth rate. This shows that 3D MHD spectroscopy can offer insights into strategies for improving stability by identifying the vulnerable aspects of such scenarios. In addition, the method highlights its potential for instability avoidance by enabling early detection of multiple modes, even before magnetic coils can measure them. The measured growth rate by the 3D MHD spectroscopy shows its reliability by exhibiting a correlation with the programmed rises in plasma beta across various high β_N and high q_{min} discharges. In addition, this method is successfully applied during rapidly evolving I_p ramp-up phases, a key part of the scenario development. By achieving reasonable growth rate measurements at high-performance scenario developments, this technique contributes to the development of advanced diagnostic tools for tokamak scenario stability, which will help identify an effective pathway to stable, high-performance scenarios.

Submitted to: Nucl. Fusion

1. Introduction

To optimize magnetic fusion performance at a manageable capital cost, tokamaks need to confine high-pressure plasmas in a compact configuration. However, operation in high-performance regimes, such as high normalized pressure (β_N) plasmas, carries a high risk of instability, because thermal and magnetic energy can drive plasma instabilities that lead to disruptions or unrecoverable degradation of energy confinement. Therefore, an efficient operation strategy in fusion reactors should focus on avoiding magnetohydrodynamic (MHD) plasma instabilities instead of trying to manage them after they arise.

Advanced tokamak (AT) scenarios, characterized by broad current density profiles and elevated minimum safety factor, represent a promising pathway for achieving the high-performance requirements of future reactors (1). These configurations enhance the coupling between the plasma and the conducting wall, thereby raising the ideal-wall MHD β_N limits. Additionally, avoiding low-order rational surfaces reduces the likelihood of longer-wavelength instabilities associated with these surfaces. Given these advantages, AT scenarios are considered promising for the design of future reactors such as EU-DEMO (2), K-DEMO (3; 4), ARIES(5), and ST pilot plant (6).

Despite these advantages, AT scenarios can remain vulnerable to MHD instabilities such as kink and tearing modes, which can degrade performance and disrupt plasmas. While first-principles modeling provides insights into these instabilities, the complexity and computational cost of these simulations make them impractical for real-time applications. Experimental detection methods, on the other hand, are typically limited to identifying instabilities after their growth, because they may not produce any detectable signals if MHD instabilities are stable and do not grow, leaving a gap in predictive capabilities to manage instabilities before they grow.

To address this gap, 3D MHD spectroscopy offers a powerful diagnostic tool by measuring plasma responses to externally applied 3D magnetic fields. Early work on closely related phenomena was carried out on DIII-D (7; 8), and this line of research was further developed in (9). Previous studies showed that measured 3D radial (Br) and poloidal (Bp) magnetic fields with magnetic sensors exhibit a clear dependence with respect to normalized beta (β_N) , even when the

applied 3D coil currents are held constant (10; 11; 12). This sensitivity arises from the interaction of the applied 3D fields with underlying MHD modes, providing a means to assess plasma stability. After the importance of multi-mode plasma response was reported in DIII-D experiments (13), multi-mode 3D active MHD spectroscopy (M3DS) (14) was developed, and the damping rate of multiple eigenmodes was extracted. This method can estimate the growth rate of both stable kink and tearing modes, which could have a significant impact on operation. In addition, recent advancements in time-domain methods have resolved the limitation of real-time applicability across various low- β_N DIII-D discharges to estimate the stability of kink and tearing mode (15; 16).

However, the application of M3DS was initially restricted to low- β_N plasmas, leaving its validation in high- β_N , high- q_{min} scenarios unexplored. Such validation is crucial, as future reactors aim to operate in these high-performance regimes where MHD stability plays a critical role in maintaining good confinement. Additionally, the first principle simulations of MHD stability become more complex and computationally more expensive in these highperformance plasmas due to the importance of nonideal effects, such as drift kinetic effect (12). This work seeks to fill this gap by validating the applicability of M3DS in high- β_N , high- q_{min} plasmas during AT scenario development. Testing and validating M3DS during the development of these scenarios is essential for ensuring the reliability of this diagnostic and control method, particularly for reactors with similar highbeta requirements.

This paper is structured as follows. Section 2 describes the M3DS model and the parameter optimization applied for the DIII-D AT scenario development. Section 3 discusses the stability challenges and potential mitigation strategies for crossing $q_{min} \sim 2$. Section 4 presents the stability evolution at high q_{min} , high β_N and during the I_p ramp-up phase to evaluate the possibility of preemptive detection of instability. Finally, Section 5 provides a summary of the main conclusions from this work and outlines directions for future work.

Matrix Dimensions Description

Matrix	Difficusions	Description
A	$N \times N$	Describes the system dynamics, where N denotes the number of
		eigenmodes in the system.
B	$N \times M$	Represents the influence of the applied 3D coil current δJ_k on the
		system, where M represent the number of coil row
C	$l \times N$	Describes the contribution of the eigenmodes' response to sensor
		measurements δB_k , where l being the number of sensor arrays.
D	$l \times M$	Represents the response of the vacuum vessel and other
		components to the applied 3D perturbations.

Table 1. Description of Matrices A, B, C, and D in the System

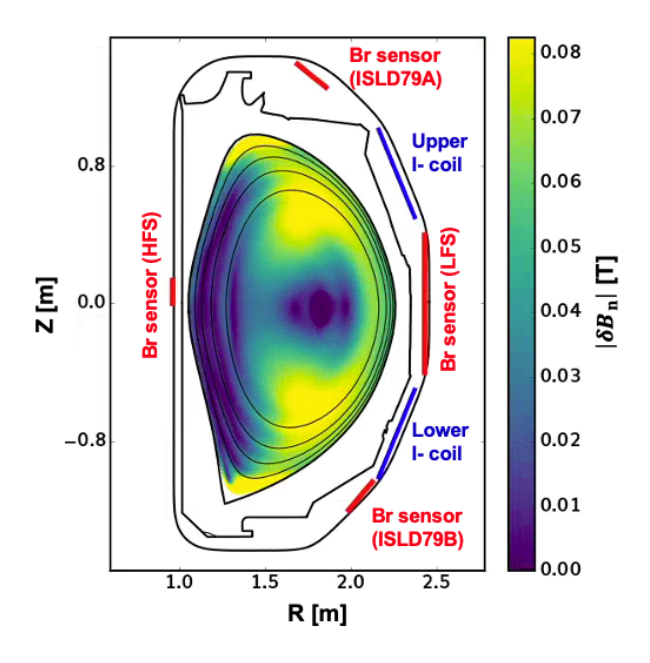


Figure 1. Schematic representation of the poloidal cross-section in a DIII-D tokamak. The color map represents the amplitude of n = 1 normal magnetic field δB_n obtained using GPEC (17) simulation (#195062 at t=3.2~s with $I_U=I_L\sim1.5$ kA and $\delta\phi \sim 330^{\circ}$), while the black contour lines indicate rational surfaces. Red markers indicate the locations of magnetic (B_r) sensors, including high-field-side (HFS) sensors, while blue markers represent the positions of upper and lower I-coils.

2. Active 3D MHD spectroscopy analysis

2.1. Model

The multi-mode 3D active MHD spectroscopy (M3DS) (14; 15; 16) in this work identifies the stability of the system using 3D coil current as an input and measured perturbed magnetic field as an output. These signals are used to identify systems using the equations (1a) and (1b),

$$\mathbf{x}_{k+1} = A\mathbf{x}_k + B\delta\mathbf{J}_k,\tag{1a}$$

$$\delta \mathbf{B}_k = C \mathbf{x}_k + D \delta \mathbf{J}_k. \tag{1b}$$

where equation (1a) represents the coupling between the external 3D coil current and the system's eigenmodes, while equation (1b) describes how measured perturbed magnetic field responds to an externally applied 3D coil current. The \mathbf{x}_k is the system state vector, and $\delta \mathbf{B}_k$, the system output, refers to the total perturbed magnetic fields measured by sensor arrays, which includes contributions from the plasma, vacuum vessel, and other structures. During experimental discharges, $\delta \mathbf{B}_k$ is measured using toroidal arrays of magnetic sensors placed at multiple poloidal locations. The vector $\delta \mathbf{J}_k$ represents the system input, which represents externally applied 3D current field perturbations. Table 1 summarizes the meaning of matrices A, B, C, and D. These matrices can be derived from linear MHD theory (14), capturing the plasma response under the influence of external 3D perturbations.

To enhance data processing, this work employs subspace system identification (SSI) theory to derive matrices in equations (1a) and (1b) that enhance numerical efficiency and convergence while offering robust resistance to noise. This approach facilitates the use of real-time signals for detecting MHD instabilities in real-time. Further details on the implementation of this approach can be found in (18; 19; 15).

2.2. Optimization

For M3DS analysis, two rows of I-coils are used in the experiment to modify the poloidal spectrum of applied n = 1 fields (n is the toroidal mode number). These are the upper and lower arrays shown in Fig. 1. The spectrum is changed by doing a coil phasing scan, $\delta \phi = \phi_{up} - \phi_{low}$, which scans various toroidal phase differences between upper and lower coil arrays as shown in Fig. 2. This phasing scan enables the identification of responses from multiple MHD eigenmodes across various sensor measurements for each phasing, as each eigenmode is characterized by a unique poloidal spectrum. Here, eigenmode refers to an MHD eigenmode from MHD energy, representing the plasma's natural response to perturbations. Extracting multiple eigenmodes through phasing scan provides a

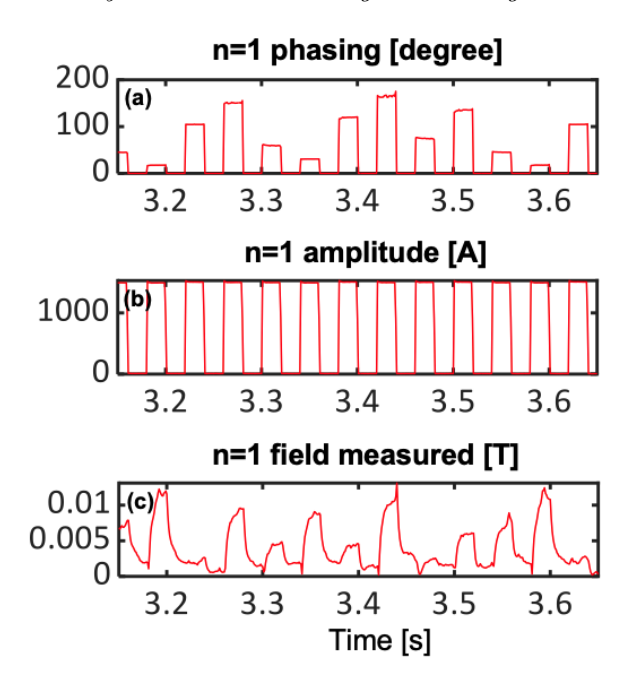


Figure 2. Time evolution of applied n=1 field (a) phasing, (b) amplitude, (c) and measure amplitude with magnetic sensors.

more precise estimation of plasma stability, eliminating the need for dedicated frequency scans (14). Based on the previous results which gave a good signal to noise ratio than other waveforms (15), the experiments used square waves which can apply multiple frequencies due to higher harmonics components in that signal. The phasing scan pattern used in this work was originally optimized for IBS scenarios (16), and the same setup was adopted here to avoid additional optimization time. Although not re-tuned for each discharge, this study can evaluate how well this configuration performs across a broader range of conditions. As shown in the following analysis, the setup remains effective and yields consistent responses, supporting its broader applicability. Although Fig. 1(c) shows that the signal does not return exactly to the baseline during the coil-off period, its relatively flat behavior suggests that this is not due to insufficient phase-hold duration but rather due to uncertainties in the magnetic signal analysis. These issues should be addressed in future work through improved signal processing techniques.

After the initial design of the 3D waveform, the experiment investigated optimal 3D current amplitudes for M3DS analysis at high $\beta_N \sim 3$. This needed an empirical scan of coil current, because resonant field amplification is harder to predict and becomes more important in high beta plasma (20; 12). To identify the optimal coil current level, the experiment compared cases without a 3D field, 800 A, and 1000 A at IU30 (I-coil in the upper row at toroidal angle 30°) as shown in Fig. 3. For example,

Figure 3 shows that the coil currents of 1000 A can sometimes result in earlier instability and unnecessary degradation of β_N . On the other hand, coil current of 800 A was shown to maintain similar plasma confinement and stability compared to the no-3Dfield cases for multiple discharges. This optimal 3D coil current induces enough signal at the magnetic sensors to provide a good enough signal-to-noise ratio while degradation in plasma confinement and stability was avoided. Therefore, coil current of 800 A was chosen and applied for the later high-beta experiments. Note that to ensure sufficient signal quality for the analysis, A coil current of 800 A was used to ensure sufficient signal quality for the analysis. While the magnetic response scales approximately linearly with the current, the noise-sensitive nature of the fitting process may lead to nonlinearly degraded accuracy at lower amplitudes. The minimum required current has not yet been validated and will be investigated through dedicated studies in future work.

Figure 4 shows the evolution of estimated plasma stability with a gradual increase of β_N . This change is driven by a slow increase in heating power starting at t = 2.4s. As a result, β_N increased from 1.8 to 3, with relatively small change of q_{min} changes from 2.6 to 2.3. Here is estimated using equilibrium reconstruction using Motional Stark Effect (MSE) diagnostics, and there is an issues of uncertainties in $q_m in$ shown in (21). However, at $t \sim 2.8 \ s$, the gradual increase in β_N halts due to the destabilization of an n = 1 MHD mode when β_N reaches around 3. This destabilization causes β_N to decrease to 2.5, even though the heating power remains unchanged. These observations indicate that the n =1 instability imposes a limit on operation at high β_N . Figure 4(c) also shows the estimated growth rate $Re(\gamma)$ using M3DS which shows a correlation with the increase of β_N and its crash. While Fig. 2 indicates that a full phasing scan spans 400 ms, we use $\Delta t = 200 \text{ms}$ fitting windows instead. This duration is sufficient to cover both resonant and non-resonant phases of the scan, while offering a balance between averaging out overly transient fluctuations and maintaining sensitivity to evolving plasma conditions within the relevant transport time scale. Unless otherwise noted (e.g., for the real-time analysis), all cases presented in this paper use these $\Delta t = 200$ ms fitting windows. Right before the onset of n = 1 mode, $Re(\gamma)$ becomes very close to zero, which indicates that plasma is approaching the stability limit due to the increase of β_N . This shows the feasibility of this approach reaching a high $\beta_N > 3$. Note that this approach is not valid during the evolution of the MHD mode, as the plasma is no longer accurately described using the linearized assumptions of our method. Due to this validity issue, the stability analysis with a sufficiently large n=1

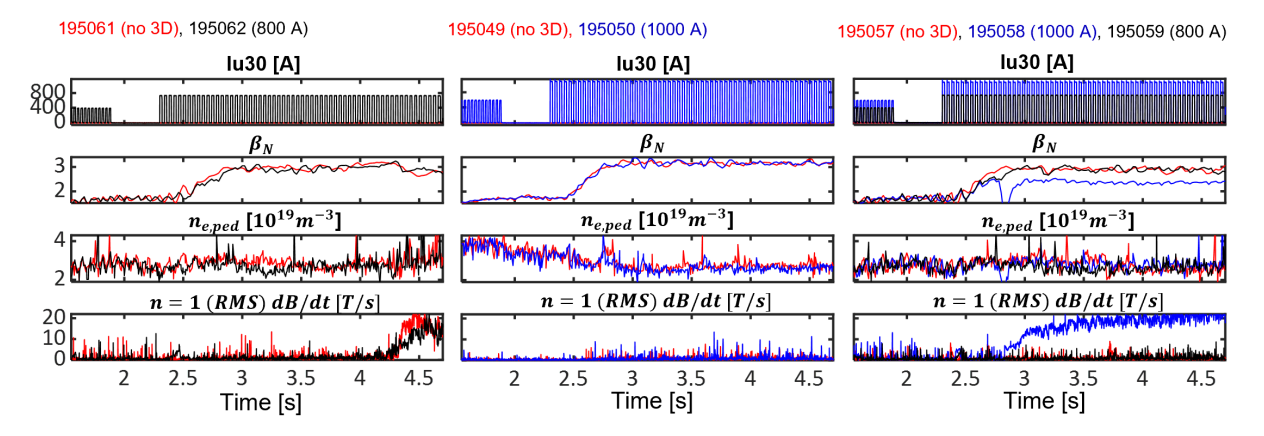


Figure 3. Time evolution of main plasma parameters under different 3D coil currents. Each column represents the same target discharge with different levels of 3D coil currents. The rows display the following time-dependent parameters: Iu30: Proxy of 3D coil current in the upper I-coil at toroidal angle 30°. β_N : Normalized beta. $n_{e,ped}$: Electron density at the pedestal. n = 1(RMS): Root mean squared (RMS) n = 1 magnetic fluctuations. Here, β_N indicates performance degradation. Also, the pedestal top density is used as a representative metric for RMP-induced density pump-out, which is expected to originate near the pedestal foot region.

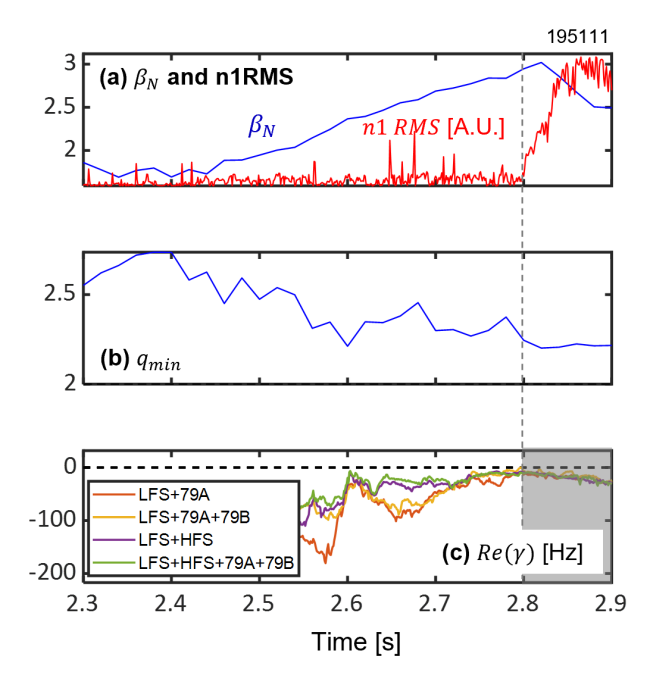


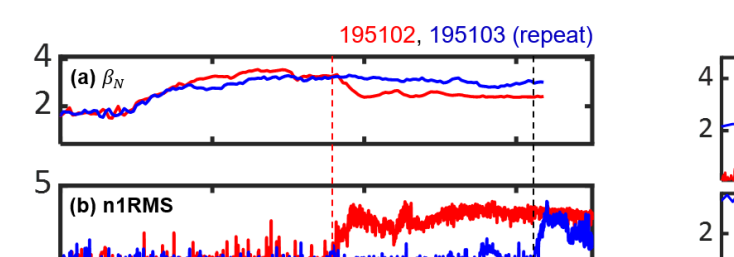
Figure 4. Time evolution of key plasma parameters during the discharge. (a) Normalized beta (β_N) shown in blue, and n=1 mode RMS amplitude (in arbitrary units, A.U.) in red, (b) minimum safety factor q_{min} evolution over time, and (c) real part of the growth rate $(\text{Re}(\gamma))$ under different sensor and magnetic sensor combinations: LFS+79A (orange), LFS+HFS (blue), LFS+79A+79B (purple), and LFS+HFS+79A+79B (green). Vertical dashed line indicates the onset of the n=1 mode.

RMS signal is grayed out in Fig. 4(c) and similar figures in the following sections.

Note that, in DIII-D, various magnetic sensors at different poloidal locations are available and the locations used in this work are shown in Fig. 1. More details of sensor locations and measurements are described in (22; 23). Figure 4 shows initial stability estimation results using a M3DS approach during the β_N evolution with different combinations of sensors. These compare four different combinations, described in Fig. 4(c). Although a general trend is not significantly different, the results without high-fieldside (HFS) sensors show some discrepancy compared with other results. Without HFS sensors, results show more oscillating variation where gradual evolution of growth rate $Re(\gamma)$ is expected during gradual β_N increase, which also agrees with results when all sensors in Fig. 4(c) are used. The importance of HFS sensors also agrees with physics intuition about efficient sensor choices to extract the various stability information from multiple eigenmodes, where the plasma's response depends on the various MHD modes. For instance, if the ballooning mode is dominant, a stronger response is expected only at the low-field-side (LFS), whereas the peeling mode is expected to produce a similar response at both the HFS and LFS. Considering these results and ideas, the analysis in the following sections used two sensors at the LFS and HFS at midplane.

3. Stability challenges and mitigation strategies when crossing $q_{min} \sim 2$

Advanced tokamak (AT) scenarios (24; 1) can be characterized by a broad current density profile and elevated q_{min} . The DIII-D tokamak is a good testbed to test AT scenarios, as it features the strong heating and current drive capabilities of DIII-D, including significant NBI power and the ability to steer EC injection from heating to direct current drive. However, maintaining $q_{min} > 2$ throughout a whole discharge in DIII-D, even with strong current drive capabilities, still remains a challenge due to loop voltage penetration



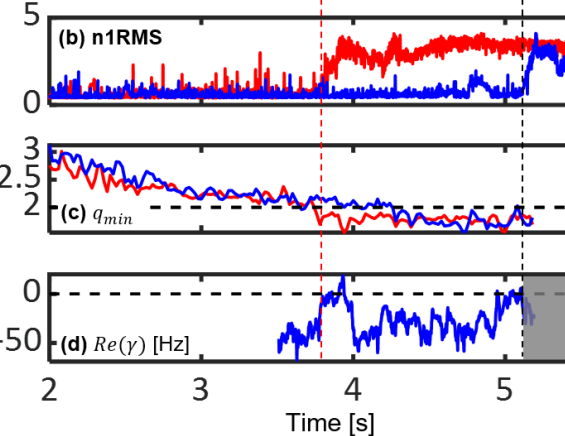


Figure 5. Time evolution of key plasma parameters during the q profile and β_N evolution. (a) Normalized beta (β_N) (b)) n=1 mode RMS amplitude (in arbitrary units, A.U.)(c) minimum safety factor q_{min} evolution over time, and (d) real part of the growth rate $(\text{Re}(\gamma))$ using LFS+HFS for discharge and 195103 (blue). There is no estimated growth rate in 195102 because the 3D field was not applied. Vertical dashed lines indicate the onset of the n=1 mode for discharges 195102 (red) and 195103 (blue).

and current profile evolution. Over time, q_{min} saturates to a lower value on the order of the current diffusion time scale. Without sufficient non-inductive current drive such as bootstrap current drive, q_{min} eventually can fall below 2 within the order of the current diffusion time scale. The emergence of additional low-order rational surfaces, such as $q_{min} \sim 2$, increases the likelihood of instabilities like tearing modes or neoclassical tearing modes (NTMs), which are associated with these surfaces.

3.1. Growth rate evolution when crossing $q_{min} \sim 2$

During the high q_{min} scenario development, MHD instabilities such as tearing modes often occur as q_{min} drops below 2. Figure 5 (195102, red) illustrates one such example, where the an n=1 instability grows at $t \sim 3.78 \, s$ with the evolution of $q_{min} \to 2$ without a big change of plasma β_N . The same discharge is repeated with a 3D field to apply M3DS analysis but this was not well reproduced with more degradation in plasma β_N . Although no instability was observed during the q_{min} crossing in another discharge (Fig. 5, 195103, blue), the detection of a positive growth rate from the M3DS analysis aligns with the emergence of n=1 mode from the reference, revealing intriguing behavior as $q_{min} \sim 2$ is crossed around $t \sim 3.78 \, s$. There is also an example

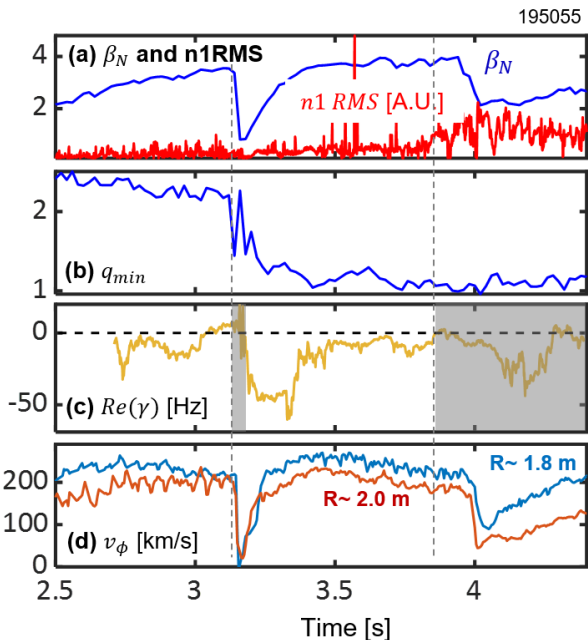


Figure 6. Time evolution of key plasma parameters during the high $\beta_N \sim 4$ discharge. (a) Normalized beta (β_N) shown in blue, and n=1 mode RMS amplitude (in arbitrary units, A.U.) in red, (b) minimum safety factor q_{min} evolution over time, (c) real part of the growth rate $(\text{Re}(\gamma))$ for the least stable mode using both LFS and HFS radial magnetic sensors, and (d) toroidal rotation at diferrent radial location. Vertical dashed lines indicate the onset of the mode locking and n=1 mode

of having locked mode when crossing $q_{min} \sim 2$ in Fig. 6(a) at $t \sim 3.1$ s which aligns with its growth rate evolution in Fig. 6(c), but this will be discussed later in the next section.

A similar intriguing dependence on q_{min} is also observed in other discharges during scenario development as shown in Fig. 7. Again, the growth rate of the least stable mode changes around $q_{min} \sim 2$ at t = 3.4 s with the appearance of an additional q=2 rational surface in this plasma. The growth rate of the least stable mode was increasing as the q=2surface emerged and decreasing at lower q_{min} . This can indicate a favorable q profile for reaching high β_N . Interestingly, the reduction of the n=1 growth rate with $q_{min} < 2$ is identified with further decrease of q_{min} even without disappearance of q=2 surfaces. During this evolution, Fig. 7(c) also shows the growth rate of the second least stable mode which behaves oppositely around $q_{min} \sim 2$ unlike the least stable mode. The growth rate goes down (2nd mode)/up (1st mode) as the q = 2 surface emerges and goes up (2nd mode)/down (1st mode) at lower q_{min} . Although the second mode appears less dominant, its evolving behavior, becoming more stable as the least stable mode grows, suggests a potential exchange in stability. Including it, therefore, could enable a more complete

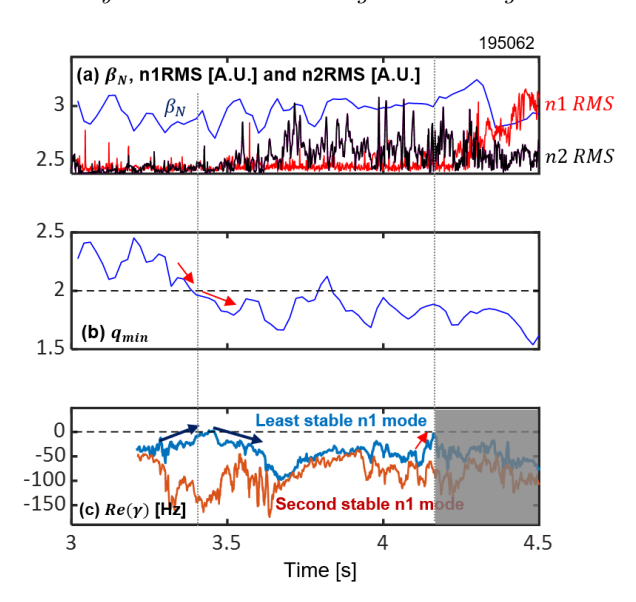


Figure 7. Time evolution of key plasma parameters during the q profile and β_N evolution. (a) Normalized beta (β_N) shown in blue, and n=1 & n=2 mode RMS amplitude (in arbitrary units, A.U.) in red, (b) minimum safety factor q_{min} evolution over time, and (c) real part of the growth rate $(\text{Re}(\gamma))$ of the n=1 mode using LFS+HFS. Vertical dotted lines indicate q_{min} crossing 2 and an increase in the growth rate before beta drop

assessment of the overall plasma response, especially in scenarios involving mode competition or nonlinear coupling.

Note that the stabilization of the least stable n=1 growth rate can also be linked to the emergence of the n=2 mode shown in Fig. 7(a), which can affect the evolution of profiles and n=1 mode (25). Some studies suggest that in a reversed magnetic shear configuration, the n=2 tearing mode is more likely to occur than n=1 mode (26). This suggests that the presence of n=2 mode, which plays a minor role in performance degradation, can suppress the more dangerous n=1 mode that significantly limits plasma performance. This is in addition to the well-known effect of a small m/n=3/2 NTM, which stabilizes the sawtooth instability by raising q_{min} slightly above 1 in the presence of low central magnetic shear (27).

In addition to this change, there is a slow increase of β_N from t=3.2 s, which leads to n=1 instability that degraded plasma β_N at around t=4.35 s. Just before the growth of the root mean square of the n=1 magnetic fluctuations (n1RMS) signal around t=4.2 s, the growth rate of the least stable mode in Fig. 7(c) exhibits a rapid increase, approaching a value near zero, which is similar to the predictive capability that will be shown in Sec. 4.1.

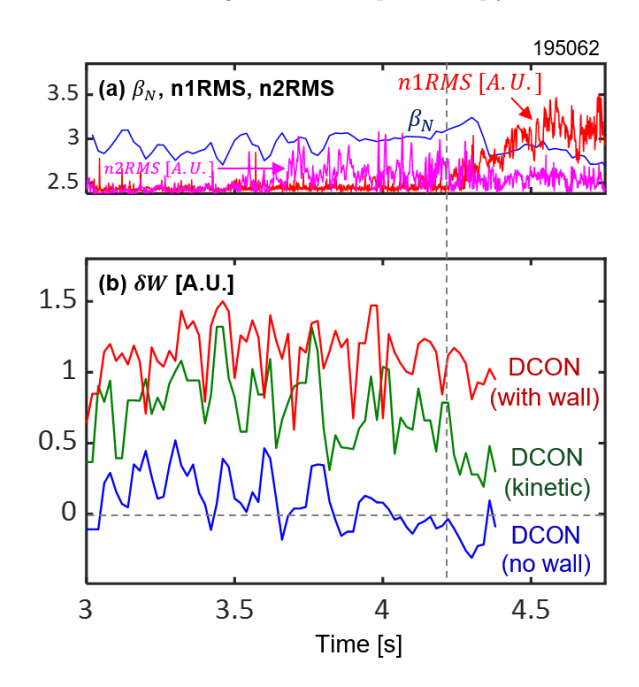


Figure 8. Time evolution of key plasma parameters during the q profile and β_N evolution. (Top) Normalized beta (β_N) shown in blue, and n=1,2 mode RMS amplitude (in arbitrary units, A.U.), (bot) δW calculated by DCON with wall effect (red line), with kinetic effects (green line), and with no wall (blue line). The dashed vertical line indicates an onset time of n=1 mode.

3.2. Analysis of underlying MHD mode

To analyze the physics of this behavior, DCON (28) stability calculations are executed for this target discharge. Figure 8 compares the evolution of δW under different conditions: with wall effects, with kinetic stabilization (29; 30), and without wall effects. The ideal MHD DCON sign convention is such that positive δW corresponds to stability (a negative growth rate). The δW is not a direct indicator of stability if kinetic effect is big because the force operator is not self-adjoint. The evolution of δW without a wall or kinetic effects shows that the plasma is getting gradually more unstable around t = 4 s without those stabilizing effects, as indicated by its sign change from positive to negative. However, the presence of wall effects and kinetic stabilization significantly alters the stability, keeping δW up at stable values even at $\beta_N \sim 3$. This comparison highlights the critical role of wall and kinetic effects in stabilizing the plasma and suggests that the observed mode is not a kink mode. Note that these DCON simulations cannot investigate tearing mode physics, as the study of tearing mode stability requires a resistivity effects.

The hypothesis that this mode is a tearing mode can be confirmed by the Beam Emission Spectroscopy (BES) signal shown in Fig. 9. Figure 9 shows a sign flip shown at a broad region around $R \sim 2.1 \ m$,

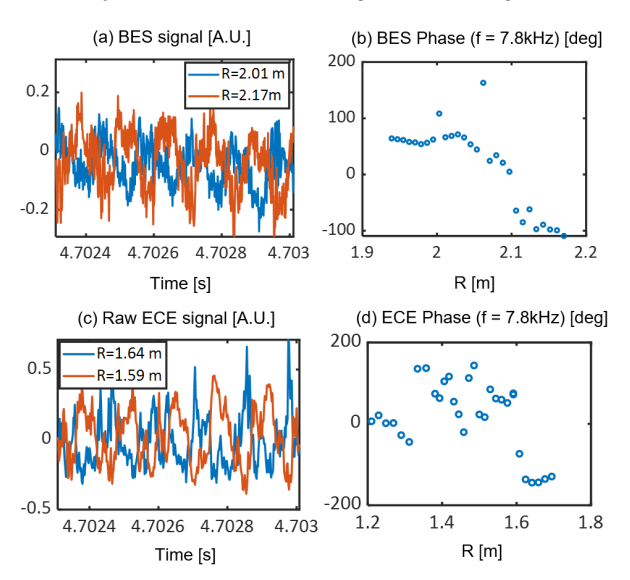


Figure 9. (a) Time evolution of BES signals at two radial positions, R=2.01 m (blue) and R=2.17 m (orange), showing opposite phases near 4.703 s. (b) Radial profile of the phase of the f=7.8 kHz component from BES. (c) Time evolution of aw ECE signals at R=1.64 m (blue) and R=1.59 m (orange), (d) phase of the f=7.8 kHz component in ECE signals as a function of R.

where the frequency of n = 1 mode is identified using analysis using Mirnov signals at frequency f = 7.8kHz around t = 4.7 s. The closest location of the rational surface is q = 2 surface, and this implies that the emergence of q=2 surface during q_{min} evolution indeed plays a role in avoiding β_N limiting n=1instabilities in this discharge. In addition, the Electron Cyclotron Emission (ECE) measurements support the presence of a tearing mode, as indicated by the phase profile shown in Fig. 9. The observed phase reversals are located on the high-field side (HFS), possibly at two radial positions, $R \sim 1.3 \ m$ and $R \sim 1.6 \ m$, which suggests the presence of a double tearing mode in this reversed magnetic shear plasma. The Mirnov analysis reveals a higher likelihood of this mode being associated with the q = 4 surface, with a chi-square value of 3.7. However, it also suggests the possibility of the mode at the q = 2 surface, although this interpretation is less supported due to the higher chisquare value of 8.05. Furthermore, the rotating tearing mode persists beyond t = 4.5 s, and β_N continues to degrade slowly during this period. This supports the interpretation that the mode remains active and influences plasma performance throughout the later phase of the discharge.

3.3. Proposed scenarios to avoid instability

Building on the observed stability evolution in high q_{min} plasmas that eventually cross $q_{min} \sim 2$, one possible strategy to manage MHD instabilities at

 $q_{min} \sim 2$ is through the controlled crossing of $q_{min} \sim$ 2 at the low- β_N stage. Unlike general operational knowledge or previous scenario-based approaches (e.g., the DIII-D hybrid scenario (27)), this strategy can be directly supported by the M3DS analysis if discharge shows stable growth rate evolution during the discharge. To validate this hypothesis we applied the M3DS approach to the case that initiated the crossing of $q_{min} \sim 2$ early in the discharge, particularly during the low- β_N stage as shown in Fig. 10. Since it covers the Ip ramp-up phase, a more detailed description of the analysis during this phase is provided in Section 4.2. As expected, Fig. 10(c) shows a very stable growth rate when crossing $q_{min} \sim 2$, unlike previous examples shown in Fig. 5 and Fig. 7. After passing this $q_{min} \sim 2$ phase, the discharge achieved $\beta_N > 3$ as shown in Fig. 10(e). This stable operation at $\beta_N > 3$ also agrees well with the stable growth rate shown in Fig. 10(g). Note that achieving $\beta_N > 3$ was much more robust in this scenario, aligning well with the approach employed in the Hybrid scenario on DIII-D (27): reducing q_{min} below 2 before raising β_N to mitigate the risk of destabilizing n=1 modes. This provides direct evidence from growth rate analysis that early crossing during the low- β_N stage can enable significantly more stable operation, highlighting the utility of the M3DS approach in scenario development. The M3DS analysis documents the strategy to cross $q_{min} \sim 2$ with improved stability, providing greater confidence in developing similar scenarios along this pathway. However, this should not be misinterpreted as a desirable feature for high- q_{min} AT scenarios, where the goal is to maintain $q_{min} > 2$ throughout the discharge. Rather, these M3DS measurements confirm the need to develop scenarios that keep q_{min} well above 2, requiring additional non-inductive current drive. Even so, the lower growth rates observed with q_{min} slightly below 2 suggest that, in certain conditions, crossing $q_{min} \sim 2$ at low beta and operating just below this threshold could help mitigate stability challenges. Additionally, the stable growth rate from M3DS results for this more reproducible low- q_{min} scenario suggests a connection between growth rate evolution and scenario reproducibility. For example, if the growth rate approaches marginal levels, it may indicate challenges in reproducing the scenario, as small changes in wall conditions or other unknown factors could introduce n = 1 instability.

As discussed in Sec. 3.1 to explain the stability behavior shown in Fig. 7, another possible approach to improving stability and avoiding the n=1 mode is to trigger higher-order modes that has a less detrimental impact on performance, such as n=3 or n=4, rather than relying on the n=2 mode, which can also degrade scenario performance in some cases. While

Stability Evaluation and Mitigation Strategies in Advanced Tokamaks using 3D MHD Spectroscopy

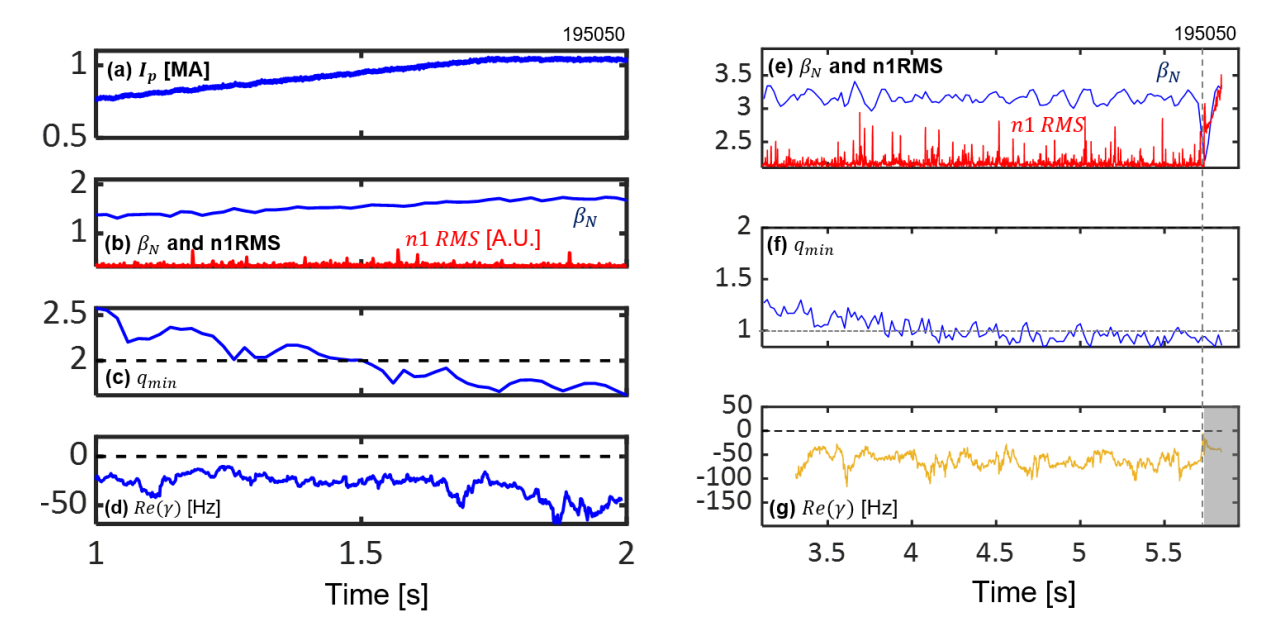


Figure 10. Time evolution of key plasma parameters during the Ip ramp up and flat-top phase of low qmin discharge: (a) Plasma current, (b) normalized beta (β_N) shown in blue, and n=1 mode RMS amplitude (in arbitrary units, A.U.) in red, (c) minimum safety factor q_{min} evolution over time, and (d) real part of the growth rate $(\text{Re}(\gamma))$ using LFS+HFS. During the flat-top phase: (e) Normalized beta (β_N) shown in blue, and n=1 mode RMS amplitude (in arbitrary units, A.U.) in red, (f) minimum safety factor q_{min} evolution over time, and (g) real part of the growth rate $(\text{Re}(\gamma))$ using LFS+HFS. Vertical dashed line indicates the onset of the n=1 mode.

the n = 2 mode is generally less disruptive than n=1, previous experiments have shown that it can still limit performance (31). The development of n=3or n = 4 modes could provide a more favorable path to maintaining stability while minimizing performance trade-offs. This makes physical sense that the highern mode takes the free energy that could potentially be taken by the n=1 mode. This strategy is similar to the hybrid scenario on DIII-D (27), which utilizes a benign m/n = 3/2 mode instead of the n = 1 mode. While the feasibility of this strategy has not been validated in this work, an analysis of high-n stability using M3DS could offer a pathway to achieving this outcome. More specifically, it would be beneficial to develop scenarios where the n = 3 growth rate approaches zero, leveraging the M3DS approach. However, further validation and optimization are required for the high-nmode analysis, which will be addressed in future work.

4. Opportunities in preemptive detection and challenges

This section documents the capability of M3DS approach in high β_N , high q_{min} regime as well as I_p ramp-up phase for its early detection of n=1 modes, which has not been studied or investigated in the previous works.

4.1. Preemptive n = 1 instability detection at high q_{min} and high β_N

Using the strong off-axis current drive capability of DIII-D q_{min} above 2 is achieved as shown in Fig. 11 and the 3D fields are applied for the M3DS analysis. In this discharge, the beta stayed at around $\beta_N \sim 2$ even with a $q_{min} > 2$ and beam power reaching 8 MW. This is due to a growth of n = 1 mode starting from $t \sim 2.8 \ s$ as indicated by an increase in the n=1RMS signal in Fig. 11(a). Interestingly, the growth rate shown in Fig. 11(c) slowly increases in time and crosses zero before the onset of the n = 1 mode observed from the n1RMS signal. The change in growth rate starts at $t \sim 2.75 \ s$, about $t \sim 0.1 \ s$ before the β_N crash at $t \sim 2.85$ s. The detection of growth rate before the β_N crash shows its capability to identify instability before it arises, providing an opportunity to implement control measures during this time. These instabilities seem to be related to the current profile evolution, which is indicated by the slow evolution of q_{min} with minor β_N change shown in Fig. 11(a).

Keeping higher β_N will be favorable for fusion reactors, but high β_N involves instability issues with increased pressure gradient and bootstrap current. Figure 6(a) shows an instabilities in the $\beta_N \sim 3.8$ discharge with initial β_N crash at $t \sim 3.1~s$ during a slow change of β_N and q_{min} . This crash is due to mode locking, which cannot be identified in the n1RMS signals that only capture rotating modes. The rapid

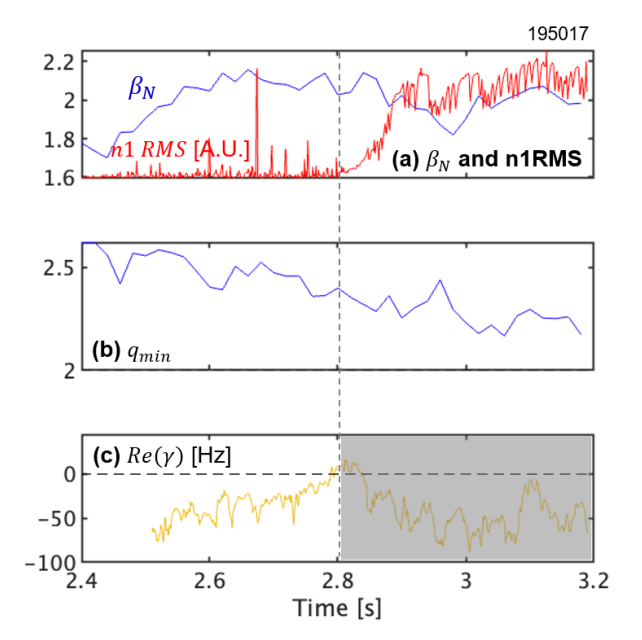


Figure 11. Time evolution of key plasma parameters during the high $q_{min}, q_{min} > 2$ discharge. (a) Normalized beta (β_N) shown in blue, and n=1 mode RMS amplitude (in arbitrary units, A.U.) in red, (b) minimum safety factor q_{min} evolution over time, and (c) real part of the growth rate $(\text{Re}(\gamma))$ for the least stable mode using both LFS and HFS radial magnetic sensors. Vertical dashed line indicates the onset of the n=1 mode.

drop in rotation to near-zero values shown in Fig. 6(d) indicates the onset of a locked mode. Since no q=2surface is present, the mode is likely a tearing mode at a higher-order rational surface, possibly corresponding to n = 3. However, identifying the mode structure after it becomes locked is challenging, as the lack of rotation hinders further mode analysis using Mirnov signals. On the other hand, the estimated growth rate shown in Fig. 6(c) captures signs of this instability. Figure 6(c) shows that the estimated growth rate becomes positive value about 0.05 second before β_N crash. The detection of near positive growth rate right before the β_N crash again shows its capability to avoid instability using detected signal using this approach. This also shows the capability of the M3DS approach that capture various frequencies that cannot be captured by the Mirnov coil due to the slow evolution of MHD mode.

A similar predictive capability was also found before a β_N crash later in time $(t \sim 3.9 \ s)$ as shown in Fig. 6(a). After the initial crash, plasma β_N recovered and reached β_N approximately 4, and plasma experienced a second drop of β_N at $t \sim 3.9 \ s$. The gradual increase of growth rate from $t \sim 3.2 \ s$ to $t \sim 3.9 \ s$ in Fig. 6(c) is found to be correlated with an increase in β_N . Also, the measured growth rate in Fig. 6(c) also becomes nearly zero before this β_N crash.

4.2. Stability estimation during Ip ramp up

The I_p ramp-up phase is a key control knob in developing AT scenarios, as it influences plasma stability and transport through the current and magnetic shear. This is due to electric field penetration during this phase and proper alignment of the electric field with plasma resistivity ensures optimal q-profile evolution, stabilizing MHD instabilities and enhancing confinement. This control is essential for developing high-performance operational regimes while avoiding harmful instabilities.

Adjusting the I_p ramp rate requires multiple discharges to test and optimize. Certain current profiles may trigger MHD instabilities, making it essential to avoid ramp rates that produce them. This optimization process can require a lot of time and resources. The use of M3DS has strong potential to provide valuable data for optimizing ramp-up scenarios. To evaluate whether M3DS can effectively track stability evolution during the I_p ramp, 3D fields are applied using an approach similar to that in Section 2. However, due to rapidly evolving plasma parameters during this phase, the 3D coil current amplitude is reduced to half its standard value. Additionally, a faster 3D coil current is used, and the duration of the phasing scan is shortened to $t=0.3\ s$ from $t=0.4\ s$.

Figure 12 shows feasibility of this approach during this ramp up phase for two different target discharges. While plasma parameters such as I_p are rapidly evolving during this time, two discharge shows quite different stability behavior. One has n = 1 MHD mode during I_p ramp up while another discharge did not have n = 1 MHD mode as shown in Fig. 12(b) and 12(e). The M3DS measured stability evolution for these discharges show quite different trend as shown in Fig. 12(d) and 12(g). Before n = 1 mode onset at around $t = 1.05 \, s$, there was an increase of growth rate approaching near zero as shown in Fig. 12(d). On the other hand, Fig. 12(g) also shows a stable growth rate during the I_p ramp-up, which agrees with the observation of no instability in the experiment. These results show its feasibility to apply this method for ramp-up phases to avoid degradation of plasma performance. Note that time scales of the M3DS analysis used same $\Delta t = 0.2 \ s$ for both I_p flat top and I_p ramp up phase, which seems to give reasonable and stable results without significant fluctuation. However, depending on the plasma evolution time scale, more optimal Δt can be found. For example, during the I_p ramp-up phase, where the plasma current is rapidly evolving, shorter I_p can be helpful to better identify the stability evolution.

Stability Evaluation and Mitigation Strategies in Advanced Tokamaks using 3D MHD Spectroscopy

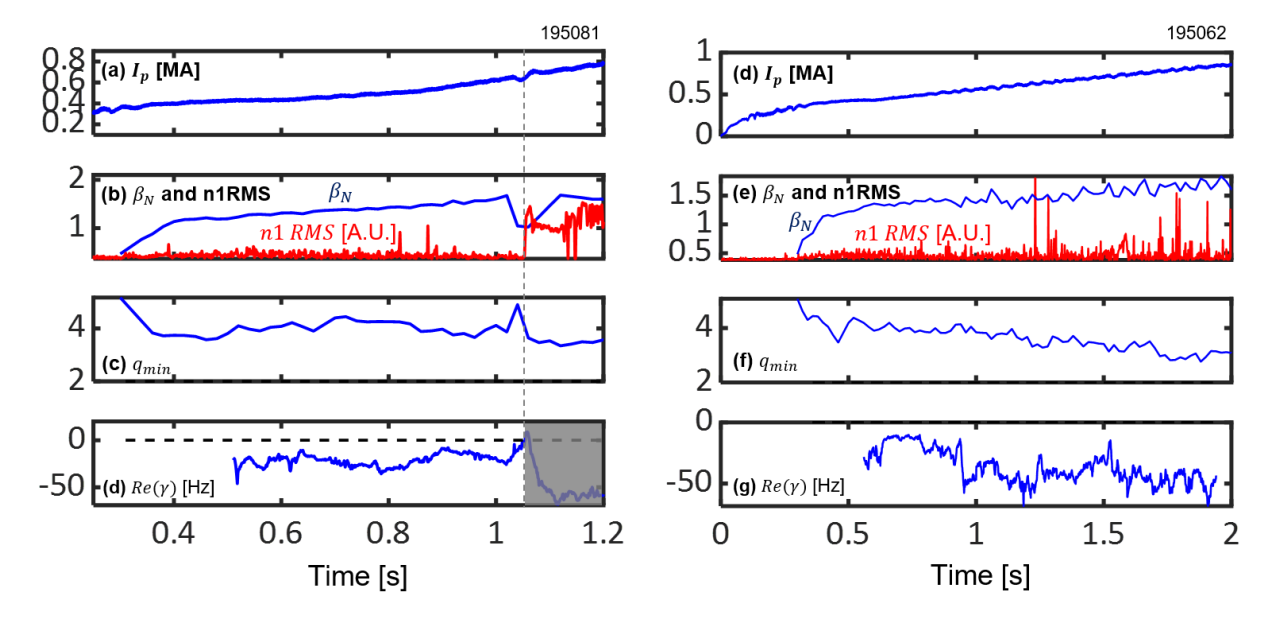


Figure 12. Time evolution of key plasma parameters during the Ip ramp up phase for two different discharges with and without n=1 MHD mode. (a,d) Plasma current, (b,e) normalized beta (β_N) shown in blue, and n=1 mode RMS amplitude (in arbitrary units, A.U.) in red, (c,f) minimum safety factor q_{min} evolution over time, and (d,g) real part of the growth rate $(\text{Re}(\gamma))$ using LFS+HFS. Vertical dashed line indicates the onset of the n=1 mode.

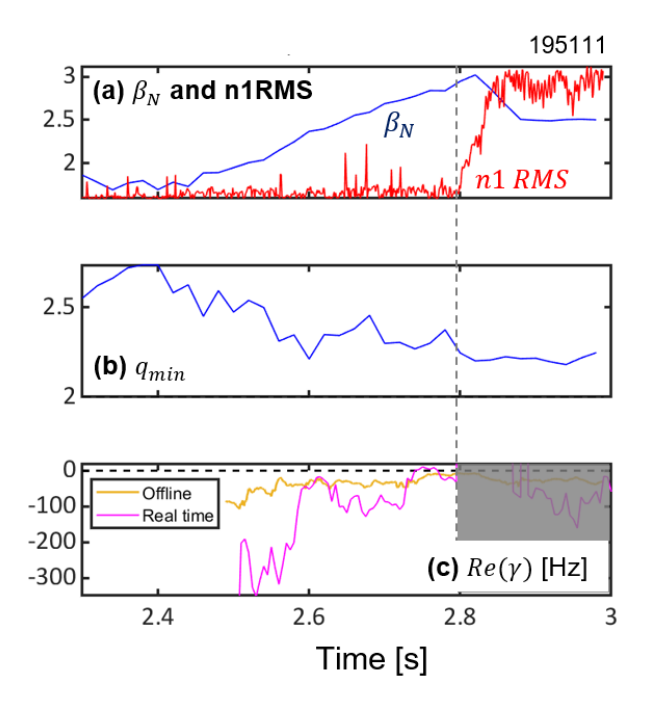


Figure 13. Time evolution of key plasma parameters during the β_N evolution. (a) Normalized beta (β_N) shown in blue, and n=1 mode RMS amplitude (in arbitrary units, A.U.) in red, (b) minimum safety factor q_{min} evolution over time, and (c) real part of the growth rate $(\text{Re}(\gamma))$ using LFS+HFS with both off line and real time analysis. Vertical dashed line indicates the onset of the n=1 mode.

4.3. Real time stability analysis

This section documents the feasibility and challenges of applying real-time stability analysis using M3DS, extending the work of Ref. (16) from low-beta plasmas. Due to computational resource limitations, the real-time analysis estimates growth rates with less information and greater uncertainties compared to offline analysis. For instance, the real-time method relies on real-time detection signals and analyzes fewer data points within a shorter time window ($\Delta t = 50 \text{ ms}$), compared to the offline analysis, which uses a longer time window ($\Delta t = 200 \text{ ms}$) for enhanced precision. The time resolution is 5 ms, and each processing cycle takes approximately 2–4 ms. The detailed setup of the real-time analysis methodology is described in (16).

Figure 13(c) compares the growth rates obtained from offline and real-time analyses during a gradual increase in β_N . Both analyses reveal an increase in growth rate over time, demonstrating the capability of the real-time approach to assess plasma stability. However, a key difference is the larger fluctuations in the real-time growth rate compared to the offline analysis, which provides more stable and less negative values. These discrepancies highlight the need for further improvements in the real-time analysis to enhance its accuracy and extend its applicability to a broader range of plasma discharges, which remains a focus for future work.

4.4. Potential limitation of the approach

2

3

4

5

6

7

8

9

10

11

12

13

14

15

16

17

18

19

20

21

22

23

24

25

26

27

28

29

30

31

32

33

34

35

36

37

38

39

40

41

42

43

44

45

46

47

48

49

50

51

52

53

54

55

56

Although MHD spectroscopy reveals intriguing behavior before instability arises in many cases, its ability to enable preemptive control can be limited in certain instances. One example is shown in Fig. 10 during the slow evolution of q_{min} around $q_{min} \sim 1$ with $\beta_N \sim 3$. In this discharge, there is a rapid increase in the n=1RMS signal at $t \sim 5.7$ s, after the emergence of the $q_{min} \sim 1$ surface. Unlike cases with slow β_N increase, the $Re(\gamma)$ before instability shows relatively rapid and transient change around the n = 1 mode onset before and after the onset. The estimated growth rate goes to near zero value with the emergence of n = 1 mode, which does not give enough time for preemptive instability control. Right before this instability, there was an unexpected event due to some impurity falling in, and this transient event eventually led to n = 1 mode. This highlights that spectroscopy cannot capture such fast changes in the plasma, as it is intended to track transport timescale evolutions. Note that this limitation is also constrained by Δt used for the M3DS analysis. For example, Δt can, in principle, be reduced to capture transient events, but this is practically difficult due to the signal to noise ratio. To improve the fitting quality, the M3DS approach requires multiple phasing scans. However, reducing Δt is limited by both the coil oscillation capabilities and the signal-to-noise ratio, which affects the quality of the fits, as illustrated by the noisier real-time (RT) results shown in Fig. 13. For example, an ELM event can become a transient source of NTM instability even at the stationary phase without a big stability change, and these instabilities are expected to be more difficult to identify in advance using this approach constrained by Δt .

5. Conclusion and future work

The study demonstrates the successful application of multi-mode active 3D MHD spectroscopy (M3DS) in developing high-beta advanced tokamak scenarios. By leveraging multiple 3D coils and magnetic sensors at different poloidal locations, experiments on the DIII-D tokamak demonstrated the method's ability to detect the growth rates of the least stable modes, correlating strongly with observed plasma instabilities across various high- β_N and high- q_{min} discharges. Unlike traditional direct coil measurements that capture perturbations only after they grow, this multimode growth rate measurement provides insight into scenario development while also enabling preemptive identification of instabilities, which can support their active control in the future.

The analysis highlighted risks of instability at integer q_{min} values (e.g., $q_{min} \sim 2$), offering insights into optimizing operation scenarios for high-

performance scenarios. The results suggest that crossing $q_{min} \sim 2$ at low β_N could offer a more stable and robust scenario, aligning with the hybrid scenario recipe. This agreement with established strategies validates both the approach and highlights the potential of applying the M3DS to pinpoint vulnerable parts in the scenario, which can also be used to devise a method to improve it. Meanwhile, these M3DS measurements also confirm the need to develop scenarios that keep q_{min} well above 2, requiring additional non-inductive current drive. Additionally, driving higher-n mode instead of n=1 mode is proposed as a potential strategy, though this requires further development of high-n M3DS approach, which remains a topic for future work.

The M3DS method also proved its predictive capability by identifying instabilities before their onset, providing opportunities for preemptive control during β_N evolution. The approach also showed its feasibility during I_p ramp-up phases, which is an important step for scenario development, by showing predictive capability by identifying instabilities before their onset. However, real-time analysis revealed some limitations in accuracy, indicating the need for further development of computational methods and tools, including more efficient calculation approaches. In addition, rapid transient events and impurity-driven instabilities posed difficulties for real-time preemptive control, as they occurred on timescales beyond the method's scope. Reducing this timescales, δt , is tied to the signal-to-noise ratio, and achieving shorter timescales while maintaining reliability requires an improved approach. In addition, while the condition $Re(\gamma) = 0$ formally defines the marginal stability boundary, in practice, identifying the precise onset of instability can be challenging because of similar uncertainty issues. These challenges will be addressed in the future through advanced signal processing using more data and machine learning (ML)-based controllers, which could enable efficient analysis of plasma stability in shorter time windows with improved accuracy. While current ML controllers lack this capability, they show promise for detecting instabilities (32). Ultimately, combining the physicsbased M3DS approach with data-driven ML controllers could overcome their limitations, enhancing both the robustness and applicability of the method.

One potential new development of M3DS could be to leverage the fitted matrices to determine the nature of the modes, utilizing the measurement of the internal structure of the 3D response. This approach would enable a more systematic and preemptive control of underlying plasma modes to enhance stability of operation. In addition, this capability can be combined with the strength of M3DS, its capacity to detect REFERENCES 13

multiple modes. For example, some modes detected from M3DS can be a favorable edge perturbations that are beneficial for edge-localized mode (ELM) control (15). By investigating the spatial structures of various modes, M3DS can help to identify the optimal 3D perturbations for ELM control, complementing existing simulation-based optimization approaches (33; 34; 35; 36).

In conclusion, the M3DS technique achieved a significant milestone by measuring growth rates at high β_N , offering actionable insights for optimizing advanced tokamak scenarios. Future research should focus on refining real-time analysis methods, which are essential for efficiently collecting a comprehensive database and studying the simultaneous detection of higher-mode behaviors such as n = 2 modes that can potentially improve the stability of n = 1 mode. Additionally, collecting more data to enable robust statistical analysis is crucial for better understanding the broader effects of this approach. Developing a machine-learning-based database will further enhance its predictive capabilities, strengthen this methodology, and contribute to reliable operation strategies for nextgeneration fusion reactors.

6. Acknowledgements

This work was supported by the U.S. Department of Energy Office of Science Office of Fusion Energy Sciences using the DIII-D National Fusion Facility, a DOE Office of Science user facilities, under Awards FC02-04ER54698, DE-AC02-09CH11466, DE-SC0022270, and DE-AC52-07NA27344. The United States Government retains a non-exclusive, paidup, irrevocable, world-wide license to publish or reproduce the published form of this manuscript, or allow others to do so, for United States Government purposes. This work is also supported by the National Magnetic Confinement Fusion Energy R&D Program (No. 2022YFE03060002)

Disclaimer: This report was prepared as an account of work sponsored by an agency of the United States Government. Neither the United States Government nor any agency thereof, nor any of their employees, makes any warranty, express or implied, or assumes any legal liability or responsibility for the accuracy, completeness, or usefulness of any information, apparatus, product, or process disclosed, or represents that its use would not infringe privately owned rights. Reference herein to any specific commercial product, process, or service by trade name, trademark, manufacturer, or otherwise does not necessarily constitute or imply its endorsement, recommendation, or favoring by the United States Government or any agency thereof. The views and

opinions of authors expressed herein do not necessarily state or reflect those of the United States Government or any agency thereof.

References

- [1] Buttery R J, Park J M, McClenaghan J T, Weisberg D, Canik J, Ferron J, Garofalo A, Holcomb C T, Leuer J and Snyder P B 2021 Nuclear Fusion 61(4) ISSN 17414326
- [2] Federici G, Kemp R, Ward D, Bachmann C, Franke T, Gonzalez S, Lowry C, Gadomska M, Harman J, Meszaros B, Morlock C, Romanelli F and Wenninger R 2014 Overview of eu demo design and rd activities Fusion Engineering and Design vol 89 (Elsevier Ltd) pp 882–889 ISSN 09203796
- [3] Kim K, Im K, Kim H C, Oh S, Park J S, Kwon S, Lee Y S, Yeom J H, Lee C, Lee G S, Neilson G, Kessel C, Brown T, Titus P, Mikkelsen D and Zhai Y 2015 Nuclear Fusion 55(5) ISSN 17414326
- [4] Kang J S, Park J M, Jung L, Kim S K, Wang J, Lee C Y, Na D H, Im K, Na Y S and Hwang Y S 2017 Nuclear Fusion 57(12) ISSN 17414326
- [5] Sorbom B N, Ball J, Palmer T R, Mangiarotti F J, Sierchio J M, Bonoli P, Kasten C, Sutherland D A, Barnard H S, Haakonsen C B, Goh J, Sung C and Whyte D G 2015 Fusion Engineering and Design 100 378–405 ISSN 09203796
- [6] Menard J E, Brown T, El-Guebaly L, Boyer M, Canik J, Colling B, Raman R, Wang Z, Zhai Y, Buxton P, Covele B, D'Angelo C, Davis A, Gerhardt S, Gryaznevich M, Harb M, Hender T C, Kaye S, Kingham D, Kotschenreuther M, Mahajan S, Maingi R, Marriott E, Meier E T, Mynsberge L, Neumeyer C, Ono M, Park J K, Sabbagh S A, Soukhanovskii V, Valanju P and Woolley R 2016 Nuclear Fusion 56(10) ISSN 17414326
- [7] Garofalo A, Strait E, Bialek J, Fredrickson E, Gryaznevich M, Jensen T, Johnson L, Haye R L, Navratil G, Lazarus E, Luce T, Makowski M, Okabayashi M, Rice B, Scoville J, Turnbull A, Walker M and Team D D 2000 Nuclear Fusion 40 1491
- [8] Okabayashi M, Bialek J, Chance M S, Chu M S, Fredrickson E D, Garofalo A M, Gryaznevich M, Hatcher R E, Jensen T H, Johnson L C, La Haye R J, Lazarus E A, Makowski M A, Manickam J, Navratil G A, Scoville J T, Strait E J, Turnbull A D, Walker M L and Team D D 2001 Physics of Plasmas 8 2071–2082 ISSN 1070-664X
- [9] Reimerdes H, Chu M S, Garofalo A M, Jackson G L, Haye R J L, Navratil G A, Okabayashi M,

REFERENCES 14

- Scoville J T and Strait E J 2004 Physical Review Letters ${\bf 93}(13)$ ISSN 00319007
- [10] Lanctot M J, Reimerdes H, Garofalo A M, Chu M S, Liu Y Q, Strait E J, Jackson G L, Haye R J L, Okabayashi M, Osborne T H and Schaffer M J 2010 Physics of Plasmas 17(3) ISSN 1070664X
- [11] King J D, Strait E J, Lazerson S A, Ferraro N M, Logan N C, Haskey S R, Park J K, Hanson J M, Lanctot M J, Liu Y, Nazikian R, Okabayashi M, Paz-Soldan C, Shiraki D and Turnbull A D 2015 Physics of Plasmas 22(7) ISSN 10897674
- [12] Wang Z R, Lanctot M J, Liu Y Q, Park J K and Menard J E 2015 Physical Review Letters 114(14) ISSN 10797114
- [13] Paz-Soldan C, Nazikian R, Haskey S R, Logan N C, Strait E J, Ferraro N M, Hanson J M, King J D, Lanctot M J, Moyer R A, Okabayashi M, Park J K, Shafer M W and Tobias B J 2015 Physical Review Letters 114(10) ISSN 10797114
- [14] Wang Z R, Logan N C, Munaretto S, Liu Y Q, Sun Y W, Gu S, Park J K, Hanson J M, Hu Q M, Strait T, Nazikian R, Kolemen E and Menard J E 2019 Nuclear Fusion 59(2) ISSN 17414326
- [15] Liu T, Wang Z R, Boyer M D, Munaretto S, Wang Z X, Park B H, Logan N C, Yang S M and Park J K 2021 Nuclear Fusion 61(5) ISSN 17414326
- [16] Liu T, Munaretto S, Logan N C, Wang Z R, Boyer M D, Wang Z X, Keith E and Park J K 2024 Nuclear Fusion 64(1) ISSN 17414326
- [17] Park J K, Boozer A H and Glasser A H 2007 Physics of Plasmas 14(5) ISSN 1070664X
- [18] Van Overschee P and De Moor B 1994 Automatica 30 75–93 ISSN 0005-1098 special issue on statistical signal processing and control
- [19] Boyer M D, Andre R, Gates D A, Gerhardt S, Goumiri I R and Menard J 2015 Nuclear Fusion 55(5) ISSN 17414326
- [20] Boozer A H 2001 Physical Review Letters **86**(22) 5059–5061 ISSN 00319007
- [21] Holcomb C T, Makowski M A, Jayakumar R J, Allen S A, Ellis R M, Geer R, Behne D, Morris K L, Seppala L G and Moller J M 2006 Review of Scientific Instruments 77 10E506 ISSN 0034-6748 URL https://doi.org/10.1063/1.2235812
- [22] King J D, Strait E J, Boivin R L, Taussig D, Watkins M G, Hanson J M, Logan N C, Paz-Soldan C, Pace D C, Shiraki D, Lanctot M J, Haye R J L, Lao L L, Battaglia D J, Sontag A C, Haskey S R and Bak J G 2014 Review of Scientific Instruments 85(8) ISSN 10897623
- [23] Munaretto S, Strait E J, Haskey S R, Logan N C, Paz-Soldan C and Weisberg D B 2018 Physics of Plasmas 25 072509 ISSN 1070-664X

- [24] Taylor T S 1997 Plasma Physics and Controlled Fusion 39 B47
- [25] Liu T, Wang J, Wei L and Wang Z X 2020 Nuclear Fusion 60 106009 URL https://dx.doi.org/10.1088/1741-4326/aba850
- [26] Liu T, Yang J F, Hao G Z, Liu Y Q, Wang Z X, Zheng S, Wang A K and He H D 2017 Plasma Physics and Controlled Fusion 59 065009 URL https://dx.doi.org/10.1088/1361-6587/aa6949
- [27] Wade M R, Luce T C, Jayakumar R J, Politzer P A, Hyatt A W, Ferron J R, Greenfield C M, Murakami M, Petty C C, Prater R, Deboo J C, Haye R J L, Gohil P and Rhodes T L 2005 Nuclear Fusion 45(6) 407–416 ISSN 00295515
- [28] Glasser A H 2016 Physics of Plasmas 23(7) ISSN 10897674
- [29] Logan N C, Park J K, Kim K, Wang Z and Berkery J W 2013 Physics of Plasmas 20 122507 ISSN 1070-664X
- [30] Park J K and Logan N C 2017 Physics of Plasmas 24(3) ISSN 10897674
- [31] Victor B, Petty C, Garofalo A M, Ding S, Shiraki D, Thome K, Holcomb C, Degrandchamp G and Chen X 2023 Progress on low-torque hybrid and high qmin scenario development on DIII-D APS Division of Plasma Physics Meeting Abstracts (APS Meeting Abstracts vol 2023) p JO08.014
- [32] Seo J, Kim S K, Jalalvand A, Conlin R, Rothstein A, Abbate J, Erickson K, Wai J, Shousha R and Kolemen E 2024 Nature 626(8000) 746–751 ISSN 14764687
- [33] Park J K, Jeon Y M, In Y, Ahn J W, Nazikian R, Park G, Kim J, Lee H H, Ko W H, Kim H S, Logan N C, Wang Z, Feibush E A, Menard J E and Zarnstroff M C 2018 Nature Physics 14(12) 1223–1228 ISSN 17452481
- [34] Yang S M, Park J K, Logan N C, Zhu C, Hu Q, Jeon Y M, In Y, Ko W H, Kim S K, Lee Y H and Na Y S 2020 Nuclear Fusion 60(9) ISSN 17414326
- [35] Yang S M, Park J K, Jeon Y M, Logan N C, Lee J, Hu Q, Lee J H, Kim S K, Kim J, Lee H, Na Y S, Hahm T S, Choi G, Snipes J A, Park G and Ko W H 2024 Nature Communications 15(1) ISSN 20411723
- [36] Kim S K, Shousha R, Yang S M, Hu Q, Hahn S H, Jalalvand A, Park J K, Logan N C, Nelson A O, Na Y S, Nazikian R, Wilcox R, Hong R, Rhodes T, Paz-Soldan C, Jeon Y M, Kim M W, Ko W H, Lee J H, Battey A, Yu G, Bortolon A, Snipes J and Kolemen E 2024 Nature Communications 15(1) ISSN 20411723